Supporting Information for

The Cyanide Ligands of [FeFe] Hydrogenase: Pulse EPR Studies of ^{13}C and ^{15}N-Labeled H-Cluster

William K. Myers, Troy A. Stich, Daniel L. M. Suess, Jon M. Kuchenreuther, James R. Swartz, R. David Britt*

Table of Contents

Materials and Methods.

In Vitro Preparation of Isotopically-Enriched [FeFe] Hydrogenase.

The CpI enzyme was post-translationally activated using previously described methods for cell-free synthesis of the H-cluster and hydrogenase maturation.[1]

In general terms, the *in vitro* maturation reaction mixture is a combination of inactive CpI apoprotein, extrinsic low-molecular weight substrates, and three *E. coli* lysates containing the HydE, HydF, and HydG maturases. Specifically, *in vitro* CpI maturation reaction mixtures (50 mL) contained 2.5 mL of HydE lysate, 5 mL of HydF lysate, 25 mL of HydG lysate, 1 mM ferrous Fe, 0.5 mM sodium sulfide, 1 mM DTT, 2 mM SAM, 2 mM L-cysteine, 2 mM L-tyrosine (natural abundance or isotopically labeled), 20 mM GTP, 1 mM PLP, 2 mM sodium dithionite, and 300 mg/L purified and desalted CpI apoprotein (5 μM). After anaerobic incubation for 24 h at 25 °C, reaction mixtures were clarified at 20000g for 10 min to remove precipitate that forms during the reaction. Active CpI was isolated from the clarified mixture using Strep-Tactin Superflow high-capacity resin (IBA GmbH), and the purified holoenzyme was concentrated to 200−600 μM. The concentrated CpI holoenzyme was stored in liquid N_2 until addition of thionin acetate within an anaerobic glovebox (100% N_2) in order to generate the H_{ox} state. Following this step, protein samples were immediately transferred to EPR tubes, removed from the glove box, and frozen using liquid N_2. For H_{ox}–CO samples, the H_{ox} sample was immediately mixed with CO-containing gas within a 3 mL syringe for 1-2 min before transferring the protein sample to the EPR tube.

Isotopically labeled L-[2-^{13}C]-tyrosine, and L-[^{15}N]-tyrosine were obtained from Cambridge Isotope Laboratories, Inc. Fresh solutions of *S*-adenosylmethionine (SAM), L-tyrosine, L-cysteine, GTP, sodium dithionite, and pyridoxal-5'-phosphate (PLP) were routinely prepared with anaerobic buffers before all *in vitro* studies. SAM was dissolved in 10% ethanol and 5 mM sulfuric acid. All other additives were dissolved in 50 mM HEPES buffer, pH 8.0.

Both the *Clostridium pasteurianum* HydA (CpI) apoprotein and the *Shewanella oneidensis* HydE, HydF, and HydG maturases were anaerobically produced in *E. coli* strain BL21(DE3) *ΔiscR::kan* using methods previously described for high-yield production of metalloproteins that contain stoichiometric amounts of Fe-S clusters.[2,3] Inactive CpI-Strep-tag II apoprotein was produced in *E. coli* grown in complex medium with natural abundance Fe (250 mg/L ferric ammonium citrate; Sigma Aldrich). HydE, HydF, and HydG were separately expressed in *E. coli* grown in complex medium. Each maturase was individually expressed in *E. coli* to prevent the *in vivo* assembly of a HydF-bound $[FeFe]_H$ precursor that can form when HydF is co-expressed with HydE and HydG.[4,5] Cell lysates were prepared using BugBuster Master Mix lysis solution (4 mL per gram of wet cell paste) supplemented with 100 mM HEPES (pH 8.2).

EPR Spectroscopy.

Continuous-wave (CW) X-band EPR spectra were collected at the CalEPR Center in the Department of Chemistry at the University of California, Davis. X-band measurements were performed with a Bruker Biospin EleXsys E500 spectrometer equipped with a cylindrical TE_{011}-mode resonator (SHQE-W), an ESR-900 liquid helium cryostat, and an ITC-5 temperature controller (Oxford Instruments). All CW EPR spectra were collected under slow-passage, non-saturating conditions. Particular spectrometer settings are given in the corresponding figure captions. Pulse X-band and Q-band HYSCORE and ENDOR measurements were performed with a Bruker Biospin EleXsys E580 spectrometer. The Q-band studies were performed using a R.A. Isaacson cylindrical TE_{011} resonator adapted from previous use[6] for pulse EPR in an Oxford Instruments CF935 cryostat. All spectra were acquired at a temperature = 20 K. The pulses sequences employed were as follows: electron spin-echo detected EPR (π/2-τ-π-τ-echo), HYSCORE (π/2-τ-π/2-t1-π-t2-π/2-τ-echo) and Mims ENDOR (π/2-τ-π /2-RF-π/2-τ-echo) and Davies ENDOR (π-RF-π/2-τ-π-τ-echo). EPR spectral simulations were performed with Matlab using the EasySpin 4.5 toolbox.[7,8]

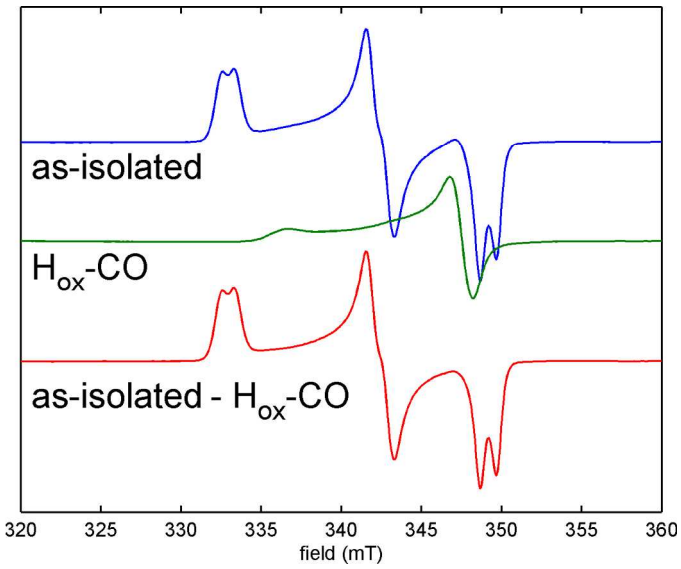

Figure S1. X-band CW EPR spectra of H_{ox} from of HydA matured with [2-^{13}C]-tyr (top); the CO-treated form of HydA (middle); and the difference spectrum (bottom) reported in Figure 1A of the main text.

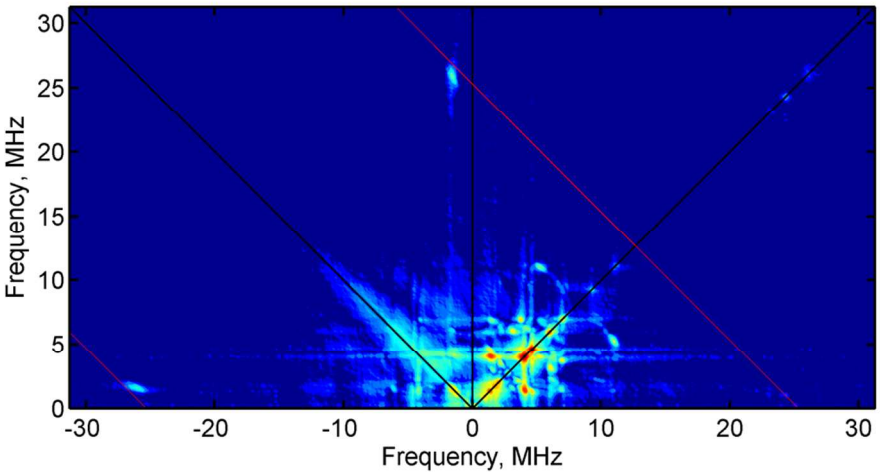

Figure S2. Q-band HYSCORE spectrum of H_{ox} ([2-^{13}C]-tyr). The red lines demarcate $y = -x \pm 2*\nu_N(^{13}C)$. The cross-peaks at (−27,+2), (−2,+27) MHz correspond to the same ^{13}C nucleus—namely the carbon of the distal CN ligand— that gives rise to the Davies ENDOR features in Figure 1B of the main text.

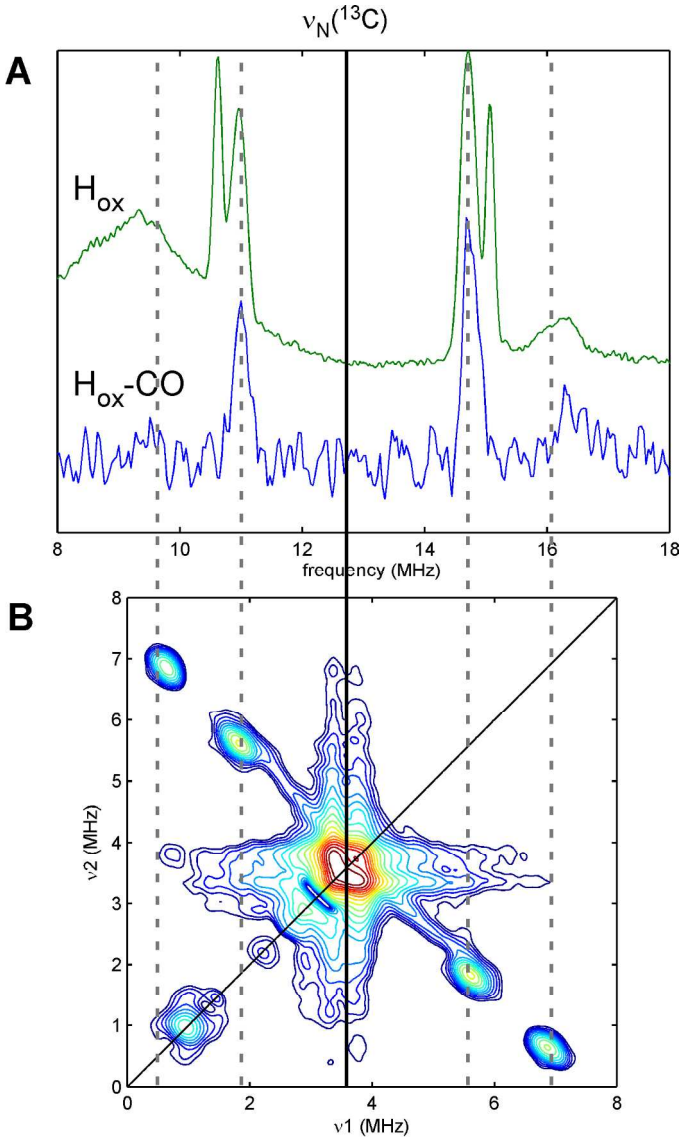

Figure S3. (**A**) Q-band Mims ENDOR spectra of HydA ([2-^{13}C]-tyr) poised in the H_{ox} state (green trace) and treated with CO (blue trace). Spectrometer settings: microwave frequency = 33.793 GHz, field = 1201.6 mT, $t_{\pi/2}$ = 20 ns, τ = 148 ns, t_{RF} = 64 µs. (**B**) X-band HYSCORE spectrum of H_{ox}–CO ([2-^{13}C]-tyr). Spectrometer settings: microwave frequency = 9.767 GHz, field = 346.8 mT, $t_{\pi/2}$ = 8 ns, τ = 136 ns. Thick vertical black line represents the ^{13}C Larmor frequency for both data sets. Dashed vertical gray lines correlate peaks due to H_{ox}–CO ([2-^{13}C]-tyr) that are observed in the ENDOR and HYSCORE spectra.

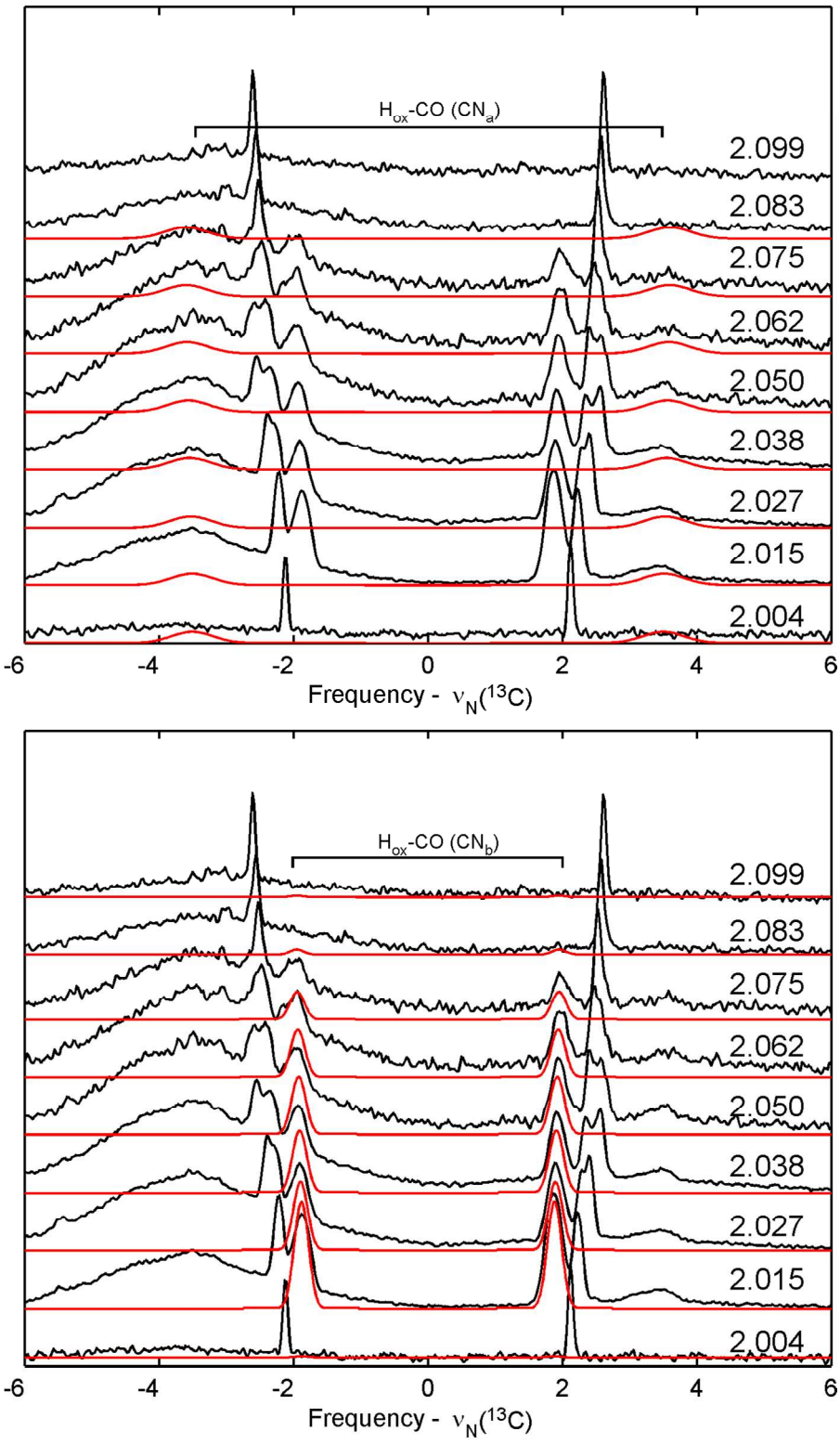

Figure S4. ^{13}C ENDOR spectral simulations (red traces) for contributions by CN_a (top) and CN_b (bottom) arising from a small contamination of H_{ox}–CO([2-^{13}C]-tyr) in the sample of H_{ox}([2-^{13}C]-tyr). Simulation parameters are reported in Table 1 and plotted over the data (black traces) originally presented in Figure 1C.

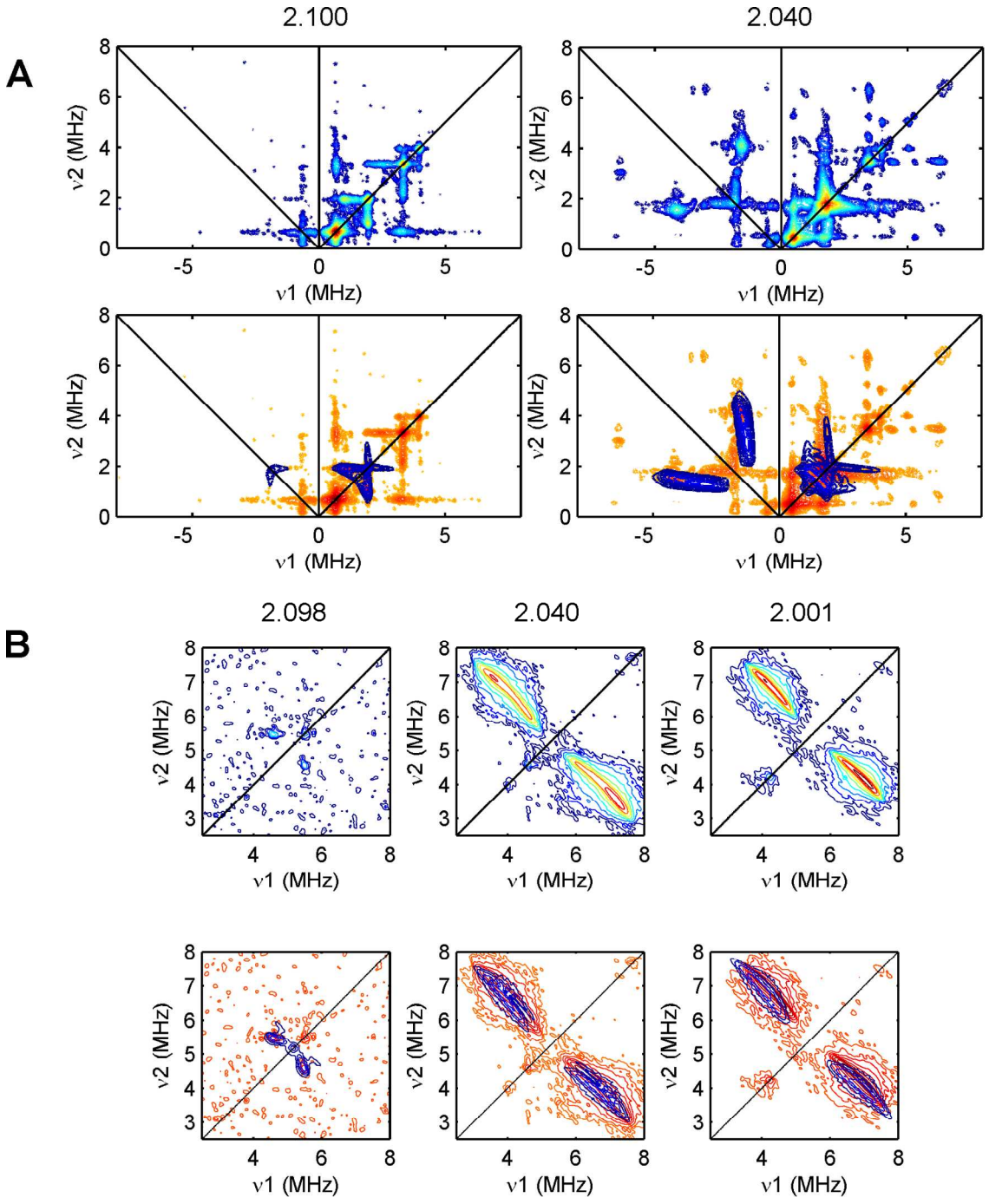

Figure S5. (**A**, top row) X-band HYSCORE spectra of H_{ox} (^{15}N-tyr) collected at 331.0 mT (left side) and 340.5 mT Spectrometer settings: microwave frequency = 9.72 GHz, $t_{\pi/2}$ = 8 ns, τ = 180 ns. (**A**, bottom row) HYSCORE spectra from top row are reproduced in red and spectral simulations obtained using best-fit parameters given in Table 1 of main text are overlaid in blue. (**B**, top row) Q-band HYSCORE spectra of H_{ox} ([^{15}N]-tyr) collected at 1160, 1181, and 1216 mT (left to right). Spectrometer settings: microwave frequency = 34.06, 33.72, and 34.06 GHz (left to right), $t_{\pi/2}$ = 24 ns, τ = 400, 388, 368 ns (left to right). (**B**, bottom row) HYSCORE spectra from top row are reproduced in red and spectral simulations obtained using best-fit parameters given in Table 1 of main text are overlaid in blue.

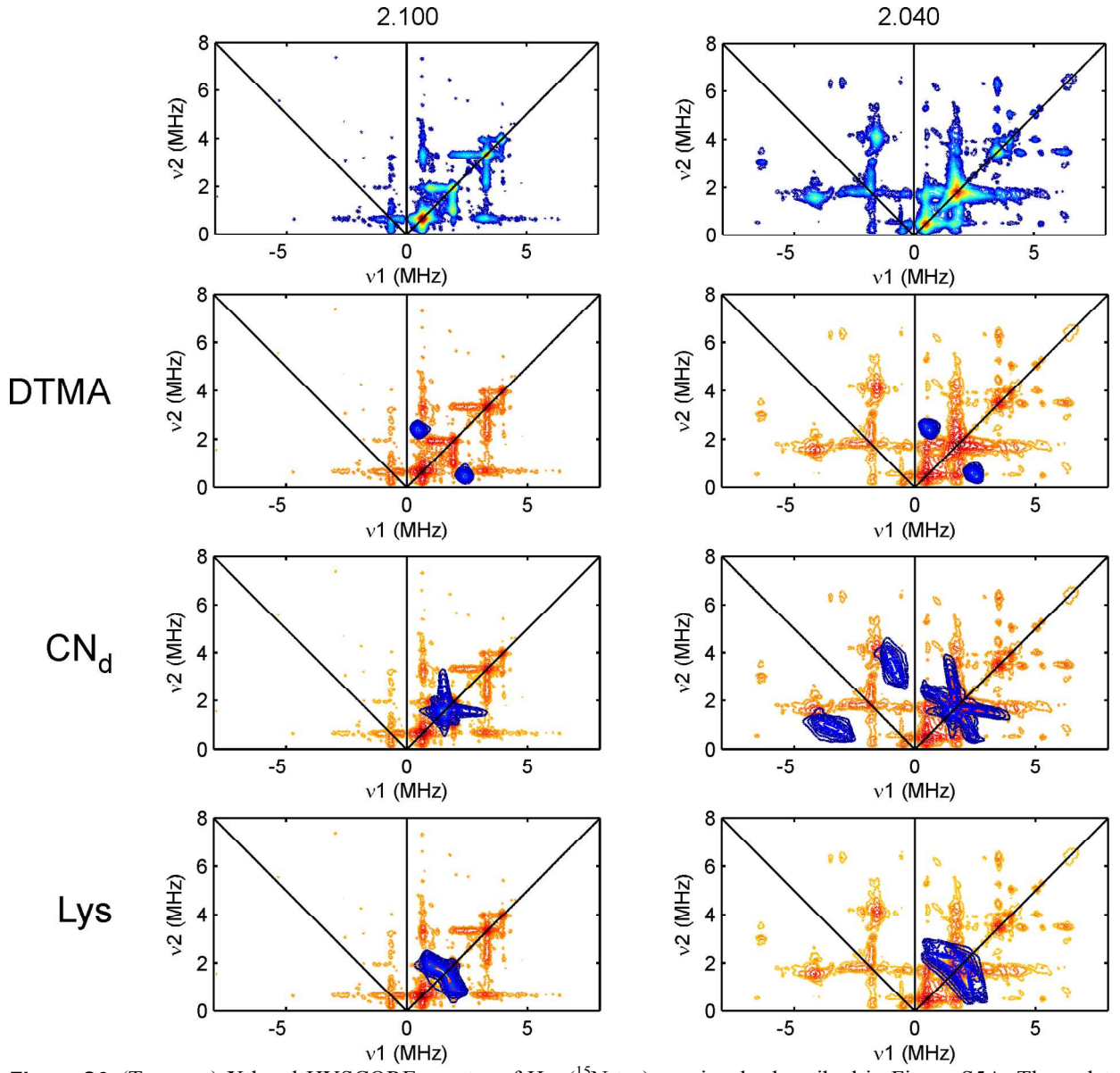

Figure S6. (Top row) X-band HYSCORE spectra of H_{ox} (^{15}N-tyr) previously described in Figure S5A. These data are reproduced in red in lower panels. Simulations are overlaid in blue and achieved using the ^{14}N HFI parameters reported in reference 9 scaled by the ratio of the ^{15}N/^{14}N Larmor frequencies (See also Table 1, main text). Specifically, row 2 illustrates the expected ^{15}N HYSCORE cross-peaks arising from the nitrogen of the DTMA ligand using the previously reported parameters. As can be seen, the predicted DTMA cross-peaks do not correspond to any features in the experimental spectrum indicating that tyrosine cannot be the source of the putative bridgehead nitrogen. Contrastingly, in row 3, we see relatively good agreement between predicted ^{15}N cross-peaks corresponding to the nitrogen of the CN bound to Fe_d and our experimental data. Unsurprisingly, the ^{15}N/^{14}N-scaled HFI assigned to a nearby lysine residue do not correspond to any ^{15}N-features in the experimental data.

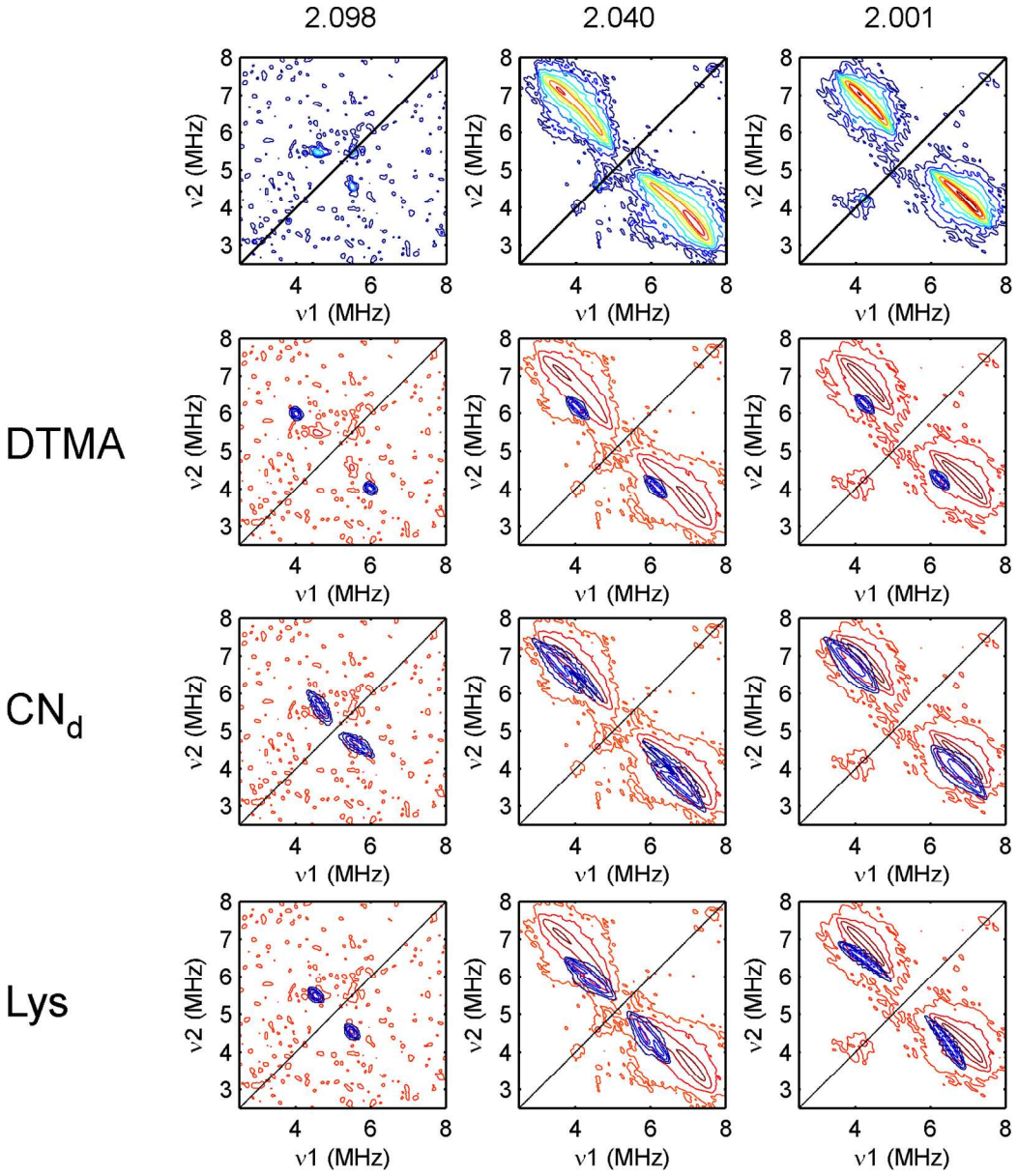

Figure S7. (Top row) Q-band HYSCORE spectra of H_{ox} (^{15}N-tyr) previously described in Figure S5B. These data are reproduced in red in lower panels. Simulations are overlaid in blue and achieved using the ^{14}N HFI parameters reported in reference 9 scaled by the ratio of the ^{15}N/^{14}N Larmor frequencies (See also Table 1, main text). Specifically, row 2 illustrates the expected ^{15}N HYSCORE cross-peaks arising from the nitrogen of the DTMA ligand using the previously reported parameters. As can be seen, the predicted DTMA cross-peaks do not correspond to any features in the experimental spectrum indicating that tyrosine cannot be the source of the putative bridgehead nitrogen. Contrastingly, in row 3, we see relatively good agreement between predicted ^{15}N cross-peaks corresponding to the nitrogen of the CN bound to Fe_d and our experimental data. Unsurprisingly, the ^{15}N/^{14}N-scaled HFI assigned to a nearby lysine residue do not correspond to any ^{15}N-features in the experimental data.

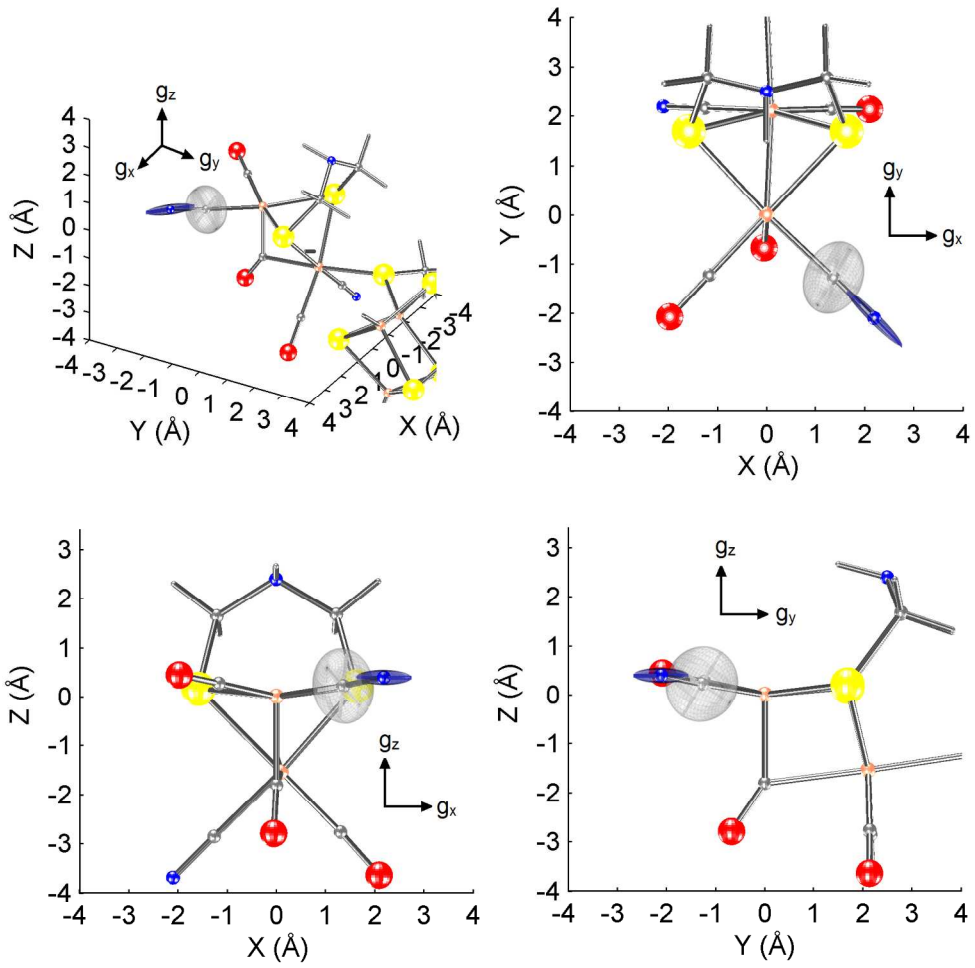

Figure S8. Different views of the ^{13}C and ^{15}N hyperfine tensors for the distal CN ligand in ellipsoid representation using the Euler angles given in Table 1. The *x*-axis was set to be collinear with a vector connecting the sulfur atoms of the DTMA ligand. The molecular *z*-axis was defined as being along the Fe–CO_{bridge} bond. Spheres represent the atoms of the $[FeFe]_H$ cluster: C (gray), N (blue), O (red), S (yellow), Fe (orange). Ellipsoid amplitudes are arbitrarily scaled.

References

(1) Kuchenreuther, J. M.; Shiigi, S. A.; Swartz, J. R. *Methods in molecular biology (Clifton, N.J.)* **2014**, *1122*, 49.
(2) Kuchenreuther, J. M.; Grady-Smith, C. S.; Bingham, A. S.; George, S. J.; Cramer, S. P.; Swartz, J. R. *Plos One* **2010**, *5*, e15491.
(3) Kuchenreuther, J. M.; Britt, R. D.; Swartz, J. R. *Plos One* **2012**, *7*, e45850.
(4) McGlynn, S. E.; Shepard, E. M.; Winslow, M. A.; Naumov, A. V.; Duschene, K. S.; Posewitz, M. C.; Broderick, W. E.; Broderick, J. B.; Peters, J. W. *FEBS Lett.* **2008**, *582*, 2183.

(5) Czech, I.; Silakov, A.; Lubitz, W.; Happe, T. *FEBS Lett.* **2010**, *584*, 638.
(6) Flores, M.; Isaacson, R. A.; Calvo, R.; Feher, G.; Lubitz, W. *Chem. Phys.* **2003**, *294*, 401.
(7) Stoll, S.; Schweiger, A. *Journal of Magnetic Resonance* **2006**, *178*, 42.
(8) Stoll, S.; Britt, R. D. *Phys. Chem. Chem. Phys.* **2009**, *11*, 6614
(9) Silakov, A.; Wenk, B.; Reijerse, E.; Lubitz, W. *PCCP* **2009**, *11*, 6592.